Nanoscale

PAPER

View Article Online
View Journal | View Issue

Cite this: *Nanoscale*, 2017, **9**, 631

Color-stable water-dispersed cesium lead halide perovskite nanocrystals†

Leyre Gomez,*[a] Chris de Weerd,[a] Jose L. Hueso[b,c] and Tom Gregorkiewicz[a]

Received 14th November 2016,
Accepted 22nd November 2016

DOI: 10.1039/c6nr08892a

www.rsc.org/nanoscale

Cesium lead halide perovskite nanocrystals are being lately explored for optoelectronic applications due to their emission tunability, high photoluminescence quantum yields, and narrow emission bands. Nevertheless, their incompatibility with polar solvents and composition homogenization driven by a fast anion-exchange are still important drawbacks to overcome. Herein we report on a successful encapsulation of colloidal perovskite nanocrystals within solid–lipid structures mainly consisting of stearic acid. The product is water-stable for a period longer than 2 months and anion-exchange is fully arrested when mixing nanocrystals of different halide compositions. This strategy boosts the potential applications of all-inorganic perovskite nanocrystals for ink-printing.

Introduction

All-inorganic perovskite nanocrystals (NCs) made of cesium lead halide ($CsPbX_3$, X = Cl, Br and I) have attracted much attention during the past year due to their emission tunability, high photoluminescence quantum yields (PL QYs = 50–90%) and narrow emission bands.[1–4] These recently discovered cubic nanoparticles combine the properties of perovskites[5,6] (high emission efficiencies and low temperature production) and quantum dots[7,8] (QDs, quantum-size effects) making them suitable for different optoelectronic applications (LEDs, solar cells, lasing).[9–14] Despite these attractive features, perovskite NCs also exhibit some important limitations, such as moisture and air instability, the presence of the toxic element lead, thermal decomposition, *etc.*[15,16] Herein, we focus our research on two major inherent drawbacks: (i) incompatibility with polar solvents and (ii) fast anion-exchange when mixed.

Colloidal perovskite NCs lose their structural integrity in the presence of polar solvents due to their inherent ionic structure and the dynamic stabilization of the surface ligands (oleylammonium bromide, oleylammonium oleate and oleylamine) which involves fast desorption.[17] There have been recent efforts to enhance their stability in air using a new surface passivation technique based on the use of an inorganic–organic ion pair, which helps to slow down the NC degradation against atmospheric moisture.[18] The use of branch-structured capping ligands has been also shown to improve their stability in polar solvents.[19] X-ray lithography has been used on NC films to form intermolecular bonds between the organic surface ligands achieving, however, only a few days of stabilization of the film immersed in Milli-Q water or buffer saline.[20] Besides, the encapsulation of QDs by micelle formation of lipid molecules[21,22] has been widely studied. Nevertheless, water-resistant $CsPbX_3$ NCs have been obtained so far only by robust non-porous coatings, such as silica spheres[23] and polyhedral oligomeric silsesquioxane[24] synthesized using water-free processes.

With an eye on optoelectronic applications, it is necessary that NCs of different compositions maintain their own emission characteristics when mixed. However, this is currently impossible as a fast anion-exchange (10–20 minutes) takes place, leading to composition homogenization.[25,26] For instance, mixing $CsPbBr_3$ and $CsPbI_3$ NCs at room temperature will yield $CsPb(BrI)_3$ NCs, and the product PL emission will be centered in between those of the initial materials. This color instability renders perovskite NCs not suitable for many imaging applications where the presence of different colors is required in order to cover the spectral range visible to the human eye.[27–29]

To overcome these limitations, here we report on the encapsulation of colloidal cesium lead halide perovskite NCs within solid lipid nanoparticles (SLNs).[30,31] SLNs are made of lipids – which are solid at room temperature – and stabilized by emulsifiers in water. They are commonly used as drug carrier

[a]*Institute of Physics, University of Amsterdam, Science Park 904, 1098 HX Amsterdam, The Netherlands. E-mail: L.gomeznavascues@uva.nl*
[b]*Institute of Nanoscience of Aragon (INA) and Department of Chemical Engineering and Environmental Technology, Edificio I+D+i, Campus Rio Ebro, 50018 Zaragoza, Spain*
[c]*Networking Research Center on Bioengineering, Biomaterials and Nanomedicine (CIBER-BBN), 28029 Madrid, Spain*

†Electronic supplementary information (ESI) available: TEM image of rod-shaped structures, photoluminescence lifetimes of $CsPbBr_3$ nanocrystals for different detection energies, photoluminescence as a function of time for colloidal nanocrystals and encapsulated perovskites dispersed in water, additional TEM images, emission peak before and after encapsulation, and emission spectra (PDF). See DOI: 10.1039/c6nr08892a

systems since they offer advantages such as a high drug payload, increased drug stability, controlled drug release, non-toxicity, feasibility of sterilization and lyophilization, and the possibility of large scale production. In addition, SLNs have already been used for the encapsulation of colloidal Si NCs[32] and Au nanoparticles[33] for fluorescence cell labeling purposes. We demonstrate that the colloidal encapsulation of perovskite NCs by SLNs renders them water-stable and arrests composition homogenization for at least 2 months, which is long enough for most applications.

Experimental

Chemicals

Cesium carbonate (Cs_2CO_3, 99.9%, Sigma-Aldrich), octadecene (ODE, 90%, Sigma-Aldrich), oleic acid (OA, 90%, Sigma-Aldrich), oleylamine (OLA, 80–90%, Acros), lead(II) bromide ($PbBr_2$, 98%, Sigma-Aldrich), lead(II) chloride ($PbCl_2$, 98%, Sigma-Aldrich), lead(II) iodide (PbI_2, 99%, Sigma-Aldrich), toluene (ACS reagent ≥99.5%, Sigma-Aldrich), stearic acid (95%, Sigma-Aldrich), and Poloxamer 188 (Kolliphor® P188, Sigma-Aldrich). All chemicals were used with no further purification, except for the drying period reported in the perovskite nanocrystal synthesis procedure.

Perovskite nanocrystal synthesis

Cesium lead halide perovskites ($CsPbX_3$) were synthesized as described by Protesescu *et al.*[1] First, Cs-oleate was prepared by mixing 0.814 g of Cs_2CO_3 with 40 mL of ODE and 2.5 mL of OA; all reactants were dried at 120 °C for 1 h. The mixture was stirred at 150 °C under a N_2 atmosphere until reaction completion was evidenced by complete dissolution of the cesium carbonate. Briefly, 5 mL of ODE and 0.188 mmol of the corresponding lead(II) halide ($PbCl_2$, $PbBr_2$, or PbI_2) were dried for 1 h at 120 °C under a N_2 atmosphere. After water removal, 0.5 mL of dried OLA and 0.5 mL of dried OA were added to the reaction flask and the temperature was raised up to 160 °C. After complete dissolution of the lead salt, 0.4 mL of the Cs-oleate solution previously warmed up was injected. A few seconds later, the NC suspension was quickly cooled down with an ice bath. The product was purified by centrifugation and redispersed in 6 mL of toluene and stored for further use.

Encapsulation of the NCs in solid–lipid structures

For an optimized and homogeneous encapsulation, 1 mL of the dispersed perovskite NCs in toluene (20 mg mL^{-1}) were mixed with 1.5 mg of stearic acid and the mixture was heated up to 75 °C in order to melt the lipid (~10 min). Thereafter, the organic dispersion was added to a water solution of 0.5 wt% P188 in the volume ratio 1 : 5 and the two phase system was sonicated for 5 min in a cold water bath (~10 °C). The microemulsion was stirred at room temperature overnight in an open vessel to let the toluene evaporate. Then, the product was washed twice by centrifugation (5000 rpm, 10 minutes) and redispersed in Milli-Q water.

Characterization

Transmission and Scanning Transmission Electron Microscopy (TEM-STEM) images were taken with a high resolution Scanning Electron Microscope (SEM, FEI Verios 460) using the STEM detector and with the aid of a FEI Tecnai F30 and an aberration-corrected FEI XFEG TITAN electron microscope operated at 300 kV using a high angle annular dark field detector equipped with a CETCOR Cs-probe corrector from CEOS Company allowing the formation of an electron probe of 0.08 nm. The geometric aberrations of the probe-forming system were controlled to allow a beam convergence of 24.7 mrad half-angle to be selected. Preliminary electron microscopy observations were completed with a T20-FEI microscope with a LaB_6 electron source fitted with a "SuperTwin®" objective lens. The sizes of the SLNs and NCs were statistically estimated by measuring the STEM and TEM images using the software ImageJ (N = 200). The optical density of the investigated colloids was measured using a LAMBDA 950 UV/Vis/NIR spectrophotometer (PerkinElmer). The PL spectra were recorded by using a Jobin Yvon FluoroLog spectrofluorometer (Horiba) equipped with a 450 W xenon lamp (250–700 nm) coupled to a monochromator, to provide a range of selected excitation wavelengths. The emission spectra were collected in a right-angle geometry and subsequently scaled for the excitation intensity, and corrected for spectral sensitivity of the detector. The PL QY has been determined using an integrating sphere with a 150 W xenon lamp coupled to a spectrometer (Solar, MSA-130) as an excitation source. The emission and excitation light is scattered diffusively in the integrating sphere and detected by using a CCD (Hamamatsu S10141-1108S) coupled to a second spectrometer (Solar, M266).[34] The picosecond PL dynamics have been measured using the frequency-doubled output of a tunable Ti:sapphire laser system (Chameleon Ultra, Coherent), providing 140 fs pulses at E_{exc} = 2.88 eV. A pulse picker has been employed to reduce the repetition rate from 80 MHz to 8 MHz. The PL emission has been detected using a monochromator (Newport CS260-02) coupled to a PMT (Hamamatsu) providing a total detection range of E_{det} = 6–1.6 eV. The overall instrument response function (IRF) was 20–25 ps (FWHM), as measured from a dilute scattering solution (Ludox) at the excitation wavelength. All measurements have been performed at room temperature.

Results and discussion

$CsPbX_3$ perovskite NCs with different halide compositions were synthesized following the procedure described by Protesescu *et al.*,[1] yielding a stable colloidal product dispersed in toluene. The absorption and emission of these perovskites can be tuned along the visible range by changing the halide composition, producing purple-, green- and red-emitting NCs (X = Cl, Br, and $Br_{0.2}I_{0.8}$, respectively, see Fig. 1a) with high PL QYs (QY_{Cl} = 52%, QY_{Br} = 85%, QY_{BrI} = 33%). In order to increase the stability of the red emitting NCs (the cubic phase of $CsPbI_3$ is typically metastable, recrystallizing into a

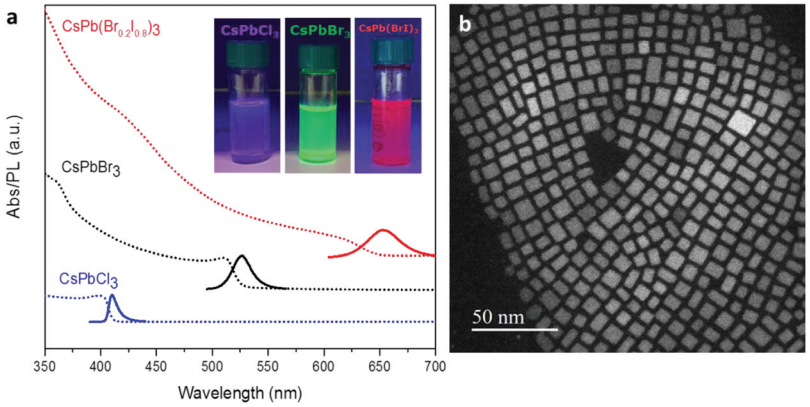

Fig. 1 (a) Absorption and photoluminescence spectra of three different halide composition perovskites $CsPbX_3$ (X = Cl, Br, $Br_{0.2}I_{0.8}$) in toluene; the inset shows the corresponding emission colors under UV lamp irradiation (365 nm). (b) STEM image of $CsPbBr_3$ nanocrystals dropcasted on a copper grid.

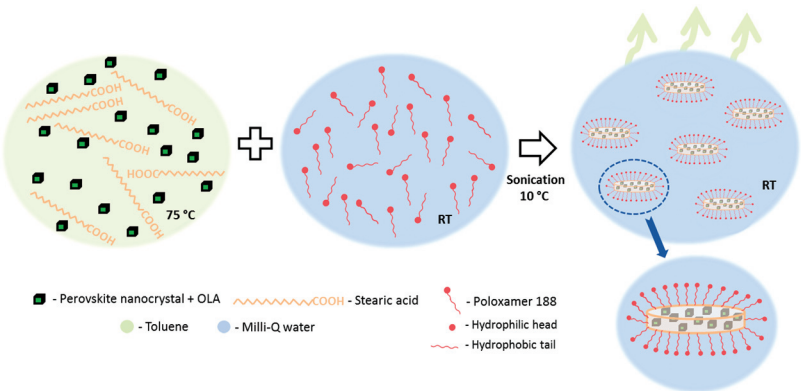

Scheme 1 Procedure for the encapsulation of $CsPbBr_3$ perovskite nanocrystals (with oleylamine as a surface ligand) in a solid lipid matrix of stearic acid by sonication-assisted melt homogenization (see the Experimental section).

non-emissive yellow phase)[35] we added 20 mol% of Br ions. $CsPbX_3$ NCs show a cubic structure (Fig. 1b) and their size can be tuned from 4 to 15 nm by the reaction temperature (140–200 °C). Nevertheless, other shape structures (rods, dots, *etc.*) can be found in the sample as subproducts of the synthesis (see ESI, Fig. 1S†). The PL lifetimes are in the order of ns as reported previously[1] (Fig. 2S†).

SLNs loaded with perovskite NCs were prepared by sonication-assisted melt homogenization (see the Experimental section and Scheme 1).[36–38] As the lipid matrix we chose stearic acid, a saturated C18 fatty acid, since it is commonly used as a drug carrier because its melting point of 69.6 °C is higher than the human body temperature.[36,37,39,40] As an emulsifier we used the surfactant Poloxamer 188 (a non-ionic triblock copolymer) without a co-surfactant. Briefly, the stearic acid was melted in a toluene solution containing the nanocrystals, and the mixture was transferred to the emulsifier water solution. Then, the two-phase suspension was sonicated in a cold water-bath to create an emulsion and to solidify the stearic acid. After toluene evaporation and sample centrifugation, the final product redispersed in Milli-Q water shows an opaque white color while the characteristic emission of the perovskite NCs can be observed under UV lamp illumination (insets in Fig. 2b and d). The SLNs with perovskite NCs were visualized by STEM and TEM showing a platelet-like shape.[30,41] The first fabrication attempt resulted in lipid structures of heterogeneous sizes, ranging from several nm to 5 μm (Fig. 2a). By subsequent adjustments and improvements in the SLN synthesis (reducing the amount of lipid and decreasing the temperature of the sonication bath), we managed to reduce the platelet size and improve the size distribution. The solid lipid platelets randomly dispersed on the TEM grid have an average size of 700 ± 240 nm (Fig. 2b). In addition, some rod-shaped particles can also be seen in Fig. 2b. As described before, these typically appear as a subproduct in the NC synthesis and can be purposefully synthesized by adjusting the reaction time and temperature.[3] When High Angle Annular Dark Field (HAADF)-STEM analysis is performed on a layered solid lipid platelet, we can see the perovskite NCs embedded in the matrix (Fig. 2c and d). We observe a decrease in the size

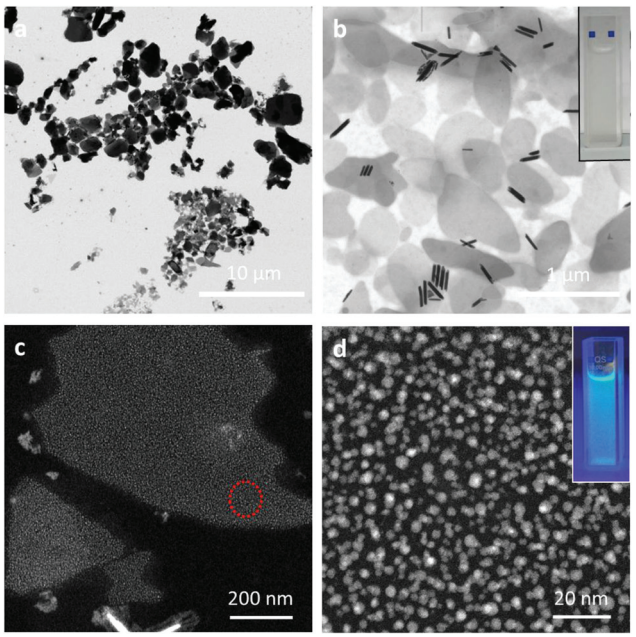

Fig. 2 (a) TEM image of a heterogeneous sample of stearic acid SLN with $CsPbBr_3$ nanocrystals inside. (b) TEM image of $CsPbBr_3$ embedded in platelet-like shape structures with an average size of 700 ± 240 nm (N = 150), some fibers can be also observed; the inset shows the sample illuminated with room light. (c) HAADF-STEM image of the perovskite nanocrystals embedded in lipid platelets. (d) HAADF-STEM zoom-in image of a lipid structure (red circle of image c) where the perovskite nanocrystals are visualized inside the matrix; the inset shows the green emission of the sample under UV lamp (365 nm) illumination.

of the NCs after the encapsulation process, from 7.2 ± 1.4 nm to 3.8 ± 0.7 nm for the green emitting sample (fresh NCs Fig. 1b and after encapsulation Fig. 2d) and the cubic shape becomes somewhat rounded up.

We compare the water-stability of free-standing and encapsulated perovskite NCs by recording the PL intensity as a function of time (Fig. 3, 3S and 4S†). Colloidal NCs in contact with Milli-Q water disintegrate within a few minutes (5–15 min) and their PL vanishes. In particular, the disintegration of $CsPbCl_3$ NCs transforms the available ions into blue emitting CsCl with a wider emission peak than the initial material (Fig. 3Sc†).[42] On the other hand, $CsPbBr_3$ and $CsPb(Br_{0.2}I_{0.8})_3$ encapsulated NCs dispersed in Milli-Q water still emit light after 2 months. The encapsulation of $CsPbCl_3$ was not successful as these NCs disintegrated before the lipid capsules were made (Fig. 4Sc,† broad emission of CsCl instead of a narrow peak from perovskite NCs). At the same time, a decrease of the NC PL intensity over time is observed, most pronounced for $CsPbBr_3$, being related with the precipitation of agglomerates. SLNs may form larger structures by the phenomenon known as gelation which can be stimulated by different situations such as insufficient stabilization, removal of the emulsifier from the particle surface by dilution, or intense contact between the SLN due to high concentration or contact with other surfaces.[30] According to our observations, storage time and exposure to an excitation source during photoluminescence experiments induce agglomeration and precipitation of the SLNs. Nevertheless, TEM and STEM images of the NCs embedded in the lipid matrix were taken 5 months after the sample was dropcasted onto the grid, showing that the NCs are still clearly visible.

After the encapsulation process, the PL maximum of the ensemble spectra blue-shifts for both, $CsPbBr_3$ and $CsPb(Br_{0.2}I_{0.8})_3$, with respect to the PL spectra of the initial dispersion of NCs in toluene (Fig. 6S†). This PL blue-shift can be explained by the earlier-mentioned size reduction of the NCs due to surface degradation during the encapsulation process. Besides the change in the NC size, a mechanical compression induced by the capsules, and/or a change in the electrical field could help to enhance the PL blue-shift.[38,43] Similar observations have been made before for micelle encapsulated quantum dots (QDs) and core–shell QDs.[44,45] The PL lifetime of the encapsulated perovskite NCs remains in the order of ns (Fig. 2S†) while the PL QY decreases after the encapsulation process (QY_{Br-SLN} = 13%, $QY_{BrI-SLN}$ = 9%). The change in the PL QY suggests NC degradation during the encapsulation process, as we have perceived from the HRTEM images. The NC degradation takes place because they are in direct contact

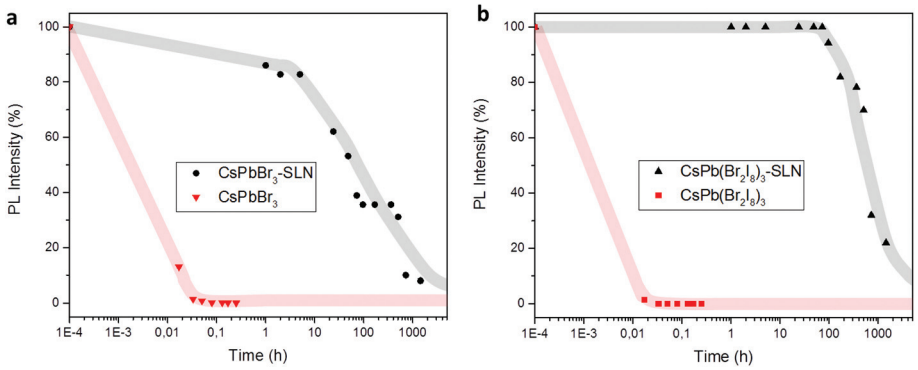

Fig. 3 Photoluminescence intensity as a function of time for free-standing (red) and encapsulated (black) $CsPbBr_3$ (a) and $CsPb(Br_{0.2}I_{0.8})_3$ (b) nanocrystals dispersed in Milli-Q water. PL intensity is normalized (100%) to the value in toluene before contact with Milli-Q water (red), and with the emission of freshly prepared encapsulated perovskites (black). The lines are a guide to the eye.

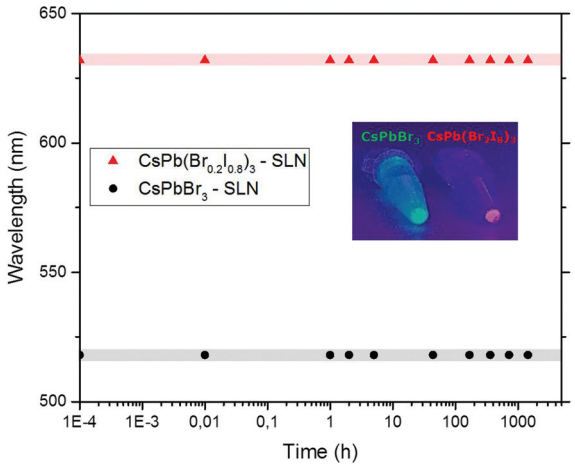

Fig. 4 Maximum peak position as a function of time for the corresponding perovskite nanocrystals' PL emission after mixing encapsulated $CsPbBr_3$ (black) and $CsPb(Br_{0.2}I_{0.8})_3$ (red) in Milli-Q water. The inset shows the emission color of the two samples under a UV lamp (365 nm).

with water until the SLN is formed. It is worth noting that the lipid matrix itself, without perovskite NCs, does not absorb light in the studied region (see Fig. 7S†).

To investigate the effect of encapsulation on anion-exchange and hence the color stability, two different types of perovskite NCs embedded in SLNs were mixed in Milli-Q water, and their PL was recorded as a function of time. As can be concluded from Fig. 4, the maximum of the emission peak of each sample ($CsPbBr_3$ – 518 nm and $CsPb(Br_{0.2}I_{0.8})_3$ – 632 nm) remains in the same position even after 2 months. This implies that composition homogenization does not take place, with the process of anion-exchange being fully arrested.

The achievement of emission and color-stable perovskite NCs enables new uses of this material. The size is sufficiently small to allow water-based ink-printing for optoelectronics[46,47] or anti-counterfeiting,[48] as nozzle diameters are typically of a few tens of micrometers. For bio-imaging purposes,[49,50] additional efforts should be carried out to further decrease the size of the platelet lipid structures. To induce a cellular response, any nanomaterial should be smaller than 100 nm, although each nanoparticle has an effective size range depending on the bio-application.[51] One way towards further size reduction could be by the influence of the surfactant type and concentration.[52]

Conclusions

Long-term emission and color stability have been demonstrated for colloidal cesium lead halide perovskite NCs dispersed in Milli-Q water. These properties have been achieved by encapsulation of perovskite NCs within SLNs of stearic acid. In this way, an easy-to-handle material, with a non-toxic carrier and free from organic solvents has been obtained. With that, the potential applications of all-inorganic cesium lead halide perovskite NCs are greatly increased; in particular, the preparation of water-based inks for jet-printing appears feasible.

Author contribution

L. G. and T. G. conceived the project and L. G. designed the experiments. L. G. synthesized the perovskite nanocrystals, and designed and carried out their encapsulation in stearic acid structures. C. W. performed the optical spectroscopy measurements. L. G. and J. L. H. acquired the TEM and STEM images. All authors discussed the results, interpreted the findings, and co-wrote the manuscript.

Competing financial interest

The authors declare no competing financial interests.

Acknowledgements

This work has been financially supported by Stichting voor Fundamenteel Onderzoek der Materie - FOM (L. G.) and by Technologiestichting STW (C. W.), The Netherlands. The authors acknowledge the FOM Institute AMOLF for the use of the FEI Verios microscope, and Dr Hong Zhang and Dr Wybren J. Buma for facilitating the ultrafast time-resolved experiments. Part of the microscopy work was conducted in the "Laboratorio de Microscopias Avanzadas" at the Instituto de Nanociencia de Aragon – Universidad de Zaragoza.

References

1 G. Nedelcu, L. Protesescu, S. Yakunin, M. I. Bodnarchuk, M. J. Grotevent and M. V. Kovalenko, *Nano Lett.*, 2015, **15**, 5635–5640.
2 A. Swarnkar, R. Chulliyil, V. K. Ravi, M. Irfanullah, A. Chowdhury and A. Nag, *Angew. Chem., Int. Ed.*, 2015, **54**, 15424–15428.
3 S. Sun, D. Yuan, Y. Xu, A. Wang and Z. Deng, *ACS Nano*, 2016, **10**, 3648–3657.
4 I. Lignos, S. Stavrakis, G. Nedelcu, L. Protesescu, A. J. deMello and M. V. Kovalenko, *Nano Lett.*, 2016, **16**, 1869–1877.
5 S. Kazim, M. K. Nazeeruddin, M. Gratzel and S. Ahmad, *Angew. Chem., Int. Ed.*, 2014, **53**, 2812–2824.
6 T. C. Sum and N. Mathews, *Energy Environ. Sci.*, 2014, **7**, 2518–2534.
7 M. G. Bawendi, M. L. Steigerwald and L. E. Brus, *Annu. Rev. Phys. Chem.*, 1990, **41**, 477–496.
8 A. P. Alisivatos, *Science*, 1996, **271**, 933–937.
9 S. Yakunin, L. Protesescu, F. Krieg, M. I. Bodnarchuk, G. Nedelcu, M. Humer, G. De Luca, M. Fiebig, W. Heiss and M. V. Kovalenko, *Nat. Commun.*, 2015, **6**, 1–8.

10 Y. Wang, X. Li, J. Song, L. Xiao, H. Zeng and H. Sun, *Adv. Mater.*, 2015, **27**, 7101–7108.
11 F. Hu, H. Zhang, C. Sun, C. Yin, B. Lv, C. Zhang, W. Yu, X. Wang, Y. Zhang and M. Xiao, *ACS Nano*, 2015, **9**, 12410–12416.
12 Y.-S. Park, S. Guo, N. S. Makarov and V. I. Klimov, *ACS Nano*, 2015, **9**, 10386–10393.
13 J. Song, J. Li, X. Li, L. Xu, Y. Dong and H. Zeng, *Adv. Mater.*, 2015, **27**, 7162–7167.
14 Y. Wang, X. Li, X. Zhao, H. Zeng and H. Sun, *Nano Lett.*, 2016, **16**, 448–453.
15 G. Niu, X. Guo and L. Wang, *J. Mater. Chem. A*, 2015, **3**, 8970–8980.
16 T. C. Jellicoe, J. M. Richter, H. F. J. Glass, M. Tabachnyk, R. Brady, S. E. Dutton, A. Rao, R. H. Friend, D. Credgington, N. C. Greenham and M. L. Böhm, *J. Am. Chem. Soc.*, 2016, **138**, 2941–2944.
17 J. De Roo, M. Ibáñez, P. Geiregat, G. Nedelcu, W. Walravens, J. Maes, J. C. Martins, I. Van Driessche, M. V. Kovalenko and Z. Hens, *ACS Nano*, 2016, **10**, 2071–2081.
18 J. Pan, S. P. Sarmah, B. Murali, I. Dursun, W. Peng, M. R. Parida, J. Liu, L. Sinatra, N. Alyami, C. Zhao, E. Alarousu, T. K. Ng, B. S. Ooi, O. M. Bakr and O. F. Mohammed, *J. Phys. Chem. Lett.*, 2015, **6**, 5027–5033.
19 B. Luo, Y.-C. Pu, S. A. Lindley, Y. Yang, L. Lu, Y. Li, X. Li and J. Z. Zhang, *Angew. Chem., Int. Ed.*, 2016, **55**, 8864–8868.
20 F. Palazon, Q. A. Akkerman, M. Prato and L. Manna, *ACS Nano*, 2016, **10**, 1224–1230.
21 B. Dubertret, P. Skourides, D. J. Norris, V. Noireaux, A. H. Brivanlou and A. Libchaber, *Science*, 2002, **298**, 1759–1762.
22 X. Gao, Y. Cui, R. M. Levenson, L. W. K. Chung and S. Nie, *Nat. Biotechnol.*, 2004, **22**, 969–976.
23 S. Huang, Z. Li, L. Kong, N. Zhu, A. Shan and L. Li, *J. Am. Chem. Soc.*, 2016, **138**, 5749–5752.
24 H. Huang, B. Chen, Z. Wang, T. F. Hung, A. S. Susha, H. Zhongb and A. L. Rogach, *Chem. Sci.*, 2016, **7**, 5699–5703.
25 G. Nedelcu, L. Protesescu, S. Yakunin, M. I. Bodnarchuk, M. J. Grotevent and M. V. Kovalenko, *Nano Lett.*, 2015, **15**, 5635–5640.
26 Q. A. Akkerman, V. D'Innocenzo, S. Accornero, A. Scarpellini, A. Petrozza, M. Prato and L. Manna, *J. Am. Chem. Soc.*, 2015, **137**, 10276–10281.
27 M. R. Luo, G. Cui and B. Rigg, *Color Res. Appl.*, 2001, **26**, 340–350.
28 E. Jang, S. Jun, H. Jang, J. Lim, B. Kim and Y. Kim, *Adv. Mater.*, 2010, **22**, 3076–3080.
29 K.-H. Lee, C.-Y. Han, H.-D. Kang, H. Ko, C. Lee, J. Lee, N. Myoung, S.-Y. Yim and H. Yang, *ACS Nano*, 2015, **9**, 10941–10949.
30 W. Mehnert and K. Mader, *Adv. Drug Delivery Rev.*, 2001, **47**, 165–196.
31 R. H. Muller, M. Radtke and S. A. Wissing, *Adv. Drug Delivery Rev.*, 2002, **54**, S131–S155.
32 E. J. Henderson, A. J. Shuhendler, P. Prasad, V. Baumann, F. Maier-Flaig, D. O. Faulkner, U. Lemmer, X. Y. Wu and G. A. Ozin, *Small*, 2011, **17**, 2507–2516.
33 G.-H. Chai, Y. Xu, S.-Q. Chen, B. Cheng, F.-Q. Hu, J. You, Y.-Z. Du and H. Yuan, *ACS Appl. Mater. Interfaces*, 2016, **8**, 5929–5940.
34 J. Valenta, *Nanosci. Methods*, 2014, **3**, 11–27.
35 A. Swarnkar, A. R. Marshall, E. M. Sanehira, B. D. Chernomordik, D. T. Moore, J. A. Christians, T. Chakrabarti and J. M. Luther, *Science*, 2016, **354**, 92–95.
36 S. Kumar and J. K. Randhawa, *RSC Adv.*, 2015, **5**, 68743–68750.
37 M. S. Baig, A. Ahad, M. Aslam, S. S. Imam, M. Aqil and A. Ali, *Int. J. Biol. Macromol.*, 2016, **85**, 258–270.
38 S. Kumar and J. K. Randhawa, *RSC Adv.*, 2014, **4**, 30186–30192.
39 E. Ugazio, R. Cavalli and M. R. Gasco, *Int. J. Pharm.*, 2002, **241**, 341–344.
40 F.-Q. Hu, S.-P. Jiang, Y.-Z. Du, H. Yuan, Y.-Q. Ye and S. Zeng, *Colloids Surf., B*, 2005, **45**, 167–173.
41 H. Bunjes, M. H. J. Koch and K. Westesen, *Langmuir*, 2000, **16**, 5234–5241.
42 P. C. Selvan and S. Selvasekarapandian, *J. Phys.: Condens. Matter.*, 1995, **7**, 5395–5404.
43 C. De Weerd, L. Gomez, H. Zhang, W. J. Buma, G. Nedelcu, M. V. Kovalenko and T. Gregorkiewicz, *J. Phys. Chem. C*, 2016, **120**, 13310–13315.
44 J. Szeremeta, L. Lamch, D. Wawrzynczyk, K. A. Wilk, M. Samoc and M. Nyk, *Chem. Phys.*, 2015, **456**, 93–97.
45 B. O. Dabbousi, J. Rodriguez-Viejo, F. V. Mikulec, J. R. Heine, H. Mattoussi, R. Ober, K. F. Jensen and M. G. Bawendi, *J. Phys. Chem. B*, 1997, **101**, 9463–9475.
46 A. Kosmala, R. Wright, Q. Zhang and P. Kirby, *Mater. Chem. Phys.*, 2011, **129**, 1075–1080.
47 J. M. Meruga, A. Baride, W. Cross, J. J. Kellar and P. S. May, *J. Mater. Chem. C*, 2014, **2**, 2221–2227.
48 C. Campos-Cuerva, M. Zieba, V. Sebastian, G. Martinez, J. Sese, S. Irusta, V. Contamina, M. Arruebo and J. Santamaria, *Nanotechnology*, 2016, **27**, 095702–095716.
49 P. Sharma, S. Brown, G. Walter, S. Santra and B. Moudgil, *Adv. Colloid Interface Sci.*, 2006, **123–126**, 471–485.
50 B. Vasudevanpillai, I. Tamitake, A. Abdulaziz, S. Athiyanathil and I. Mitsuru, *Anal. Bioanal. Chem.*, 2008, **391**, 2469–2495.
51 W. Jiang, B. Y. S. Kim, J. T. Rutka and W. C. W. Chan, *Nat. Nanotechnol.*, 2008, **3**, 145–150.
52 S. Tcholakova, N. D. Denkov and T. Danner, *Langmuir*, 2004, **20**, 7444–7458.